Progress In Electromagnetics Research C, Vol. 26, 111–121, 2012

NOVEL CAPACITIVE GAP-COUPLED BANDPASS FILTER USING NON-UNIFORM ARBITRARY IMAGE IMPEDANCE

D.-J. Jung* **and K. Chang**

Department of Electrical and Computer Engineering, Texas A&M University, College Station 77843-3128, USA

Abstract—This paper introduces a new design technique for a capacitive gap-coupled bandpass filter (BPF) using non-uniform arbitrary image impedances. Based on the proposed BPF equivalent circuit model, the filter's design equations are derived, and they are validated from comparisons of the calculated and simulated results. For this theoretical verification, the BPF using non-uniform arbitrary image impedances is designed using the specifications of: center frequency (f_c) = 5.8 GHz, fractional bandwidth (FBW) = 3.5%, and filter stage (N) = 3. The calculated and simulated results of the designed filter show good agreement. The BPF using the proposed design method could provide an advantage that one can arbitrarily determine two different image impedances, which ultimately affects the BPF's coupling gaps and line widths. This could result in suitable filter dimensions, i.e., gaps and line width, for a conventional low resolution photolithography fabrication although a low or high dielectric constant substrate is used for the design.

1. INTRODUCTION

In RF/microwave and millimeter wave systems, a filter is one of the important components since it controls signal flows within a certain frequency band. For emerging multiband/multifunction communication systems, filter designs including low loss, compact size, and high frequency selectivity are necessary. Planar type filters using microstrip have been popular, and their various design techniques have been presented for last few decades [1–16]. In planar type bandpass filters (BPFs), parallel and capacitive gap-coupled line BPFs

Received 24 October 2011, Accepted 30 November 2011, Scheduled 12 December 2011
* Corresponding author: Dong-Jin Jung (dongjin3558@neo.tamu.edu).

are frequently used for many system designs because they are relatively easy to design and provide a reasonable performance. Their analysis and design formulas are well described in [1–3]. In the designs of these microstrip coupled type BPFs, a dielectric constant should properly be selected in order to obtain suitable filter dimensions which are appropriate for a conventional low resolution photolithography fabrication process. For an example, in a conventional capacitive gap-coupled line BPF design, the lower the dielectric constant is used, the narrower the coupled-gap dimensions is required in order to obtain a desired capacitance value. Therefore, in a low dielectric constant substrate, the coupled line's gap dimension can be too narrow to be fabricated using the conventional low resolution etching process. In order to avoid the inappropriate gap dimensions, an alternative design technique to control the gap dimensions is necessary.

In [4], a parallel coupled line BPF design using a uniform arbitrary image impedance has been introduced. In this paper, a novel design technique for a capacitive gap-coupled BPF using non-uniform arbitrary image impedances is introduced. Proposed design formulas are validated from comparisons of computed and simulated data.

Using the proposed design technique, capacitive coupled line's gap dimensions can be controlled by changing the coupled line's image impedances.

2. PROPOSED DESIGN METHOD USING NON-UNIFORM ARBITRARY IMAGE IMPEDANCES

A conventional capacitive gap-coupled BPF is presented in Figure 1(a). As shown in Figure 1(a), each resonator's characteristic impedance and input/output port characteristic impedance are set at Z_o. However, the proposed capacitive gap-coupled BPFs in Figures 1(b) and (c) employ two different image impedances (Z_1 and Z_2) which are not identical to the input/output port characteristic impedances. Here, the two image impedances could arbitrarily be determined.

Figure 2 presents the equivalent circuit models of the proposed capacitive gap-coupled BPFs in Figures 1(b) and (c). It should be noted that another transmission line section at input/output in Figures 1(b) and (c) is added for maintaining symmetric coupling structures. In order to utilize admittance inverters, the equivalent circuit in Figure 2(a) could be transformed as Figure 2(b). Then, the transmission line electrical lengths in Figures 2(a) and (b) can be expressed as:

$$\theta_0 = \phi + \phi_{01} \tag{1}$$

$$\theta_i = \phi_{i-1,i} + 2\phi + \phi_{i,i+1} \tag{2}$$

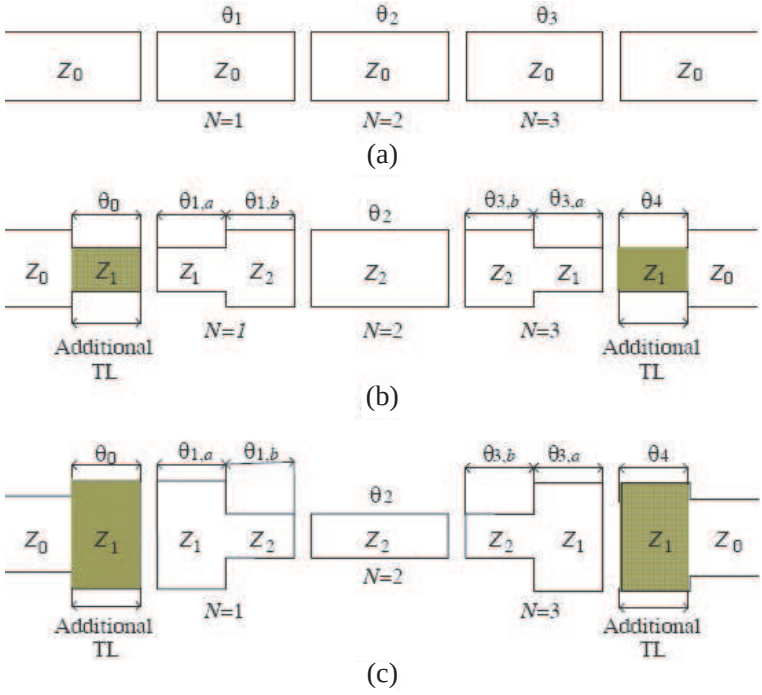

Figure 1. Capacitive gap-coupled BPFs ($N = 3$), (a) conventional BPF, (b) proposed BPF for $Z_1 > Z_2$, and (c) proposed BPF for $Z_1 < Z_2$.

where i =1, 2, 3 and ϕ =$\pi/2$ at ω_0. Electrical lengths, $\theta_{1,a}(= \theta_{3,a})$ and $\theta_{1,b}(= \theta_{3,b})$ are also expressed as $\phi_{01} + \phi$ and $\phi_{12} + \phi$, respectively.

Using the admittance inverter equivalent circuit, Figure 2(b) can be presented as Figure 2(c). Input admittance, Y_a in Figure 2(c) can be rewritten as:

$$Y_a = Y_1 \left\{ \frac{Y_1 - jY_0 \frac{1}{\tan\left(\frac{\pi}{2}\frac{\omega}{\omega_o}\right)}}{Y_0 - jY_1 \frac{1}{\tan\left(\frac{\pi}{2}\frac{\omega}{\omega_o}\right)}} \right\} = Y_1 \left\{ \frac{Y_1 + jY_o \tan\left(\frac{\pi}{2}\frac{\omega}{\omega_o} - \frac{\pi}{2}\right)}{Y_o + jY_1 \tan\left(\frac{\pi}{2}\frac{\omega}{\omega_o} - \frac{\pi}{2}\right)} \right\} \quad (3a)$$

In (3a), ω_0 is a center frequency of a designing BPF. When $\omega \approx \omega_0$, the equation in (3a) is then manipulated as:

$$Y_a = Y_1 \left\{ \frac{\frac{Y_1}{Y_o} + j\frac{\pi}{2}\left(\frac{\omega-\omega_o}{\omega_o}\right)}{1 + j\frac{\pi}{2}\frac{Y_1}{Y_o}\left(\frac{\omega-\omega_o}{\omega_o}\right)} \right\} \Bigg|_{\omega\approx\omega_o} \quad (3b)$$

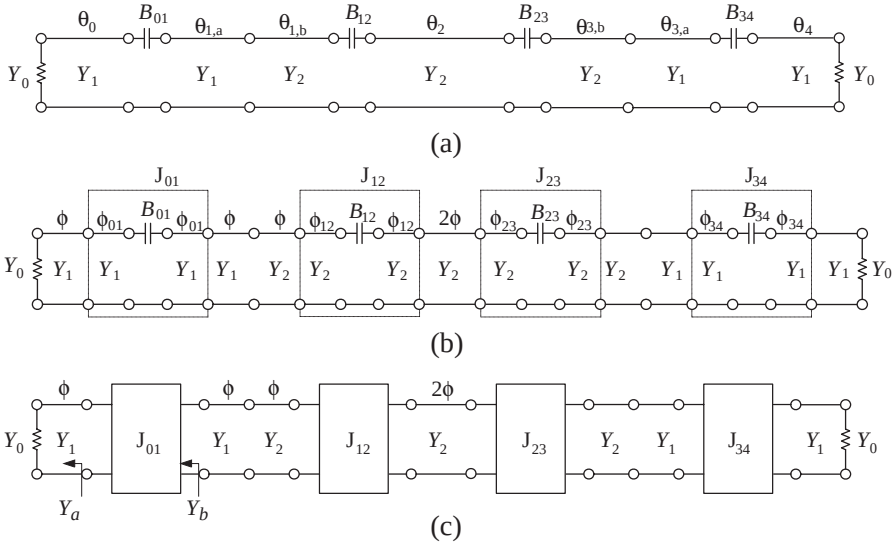

Figure 2. Equivalent circuit models of Figures 1(b) and (c), (a) transmission line model, (b) J-inverter equivalent circuit model, and (c) J-inverter model.

For simplicity, the expression in (3b) could be rewritten as:

$$Y_a = \frac{Y_1^2}{Y_o} + jY_1N\left(1 - M^2\right) \tag{4}$$

where M and N are:

$$M = \frac{Y_1}{Y_o} \tag{5}$$

$$N = \frac{\pi}{2}\left(\frac{\omega - \omega_o}{\omega_o}\right) \tag{6}$$

Based on (4), input admittance, Y_b in Figure 2(c) can be expressed as:

$$\begin{aligned} Y_b &= \frac{J_{01}^2}{Y_a} = \frac{J_{01}^2}{Y_1M + jY_1N\left(1 - M^2\right)} \\ &= \frac{J_{01}^2}{Y_1}\left\{\frac{1}{M} + jN\left(1 - \frac{1}{M^2}\right)\right\} \end{aligned} \tag{7}$$

Since the expression in (7) shows a similar form to (4), the equivalent circuit model in Figure 2(c) could be transformed as in Figure 3. As a result, B_b in Figure 3 is written as:

$$B_b = \frac{J_{01}^2 N}{Y_1}\left(1 - \frac{1}{M^2}\right) \tag{8}$$

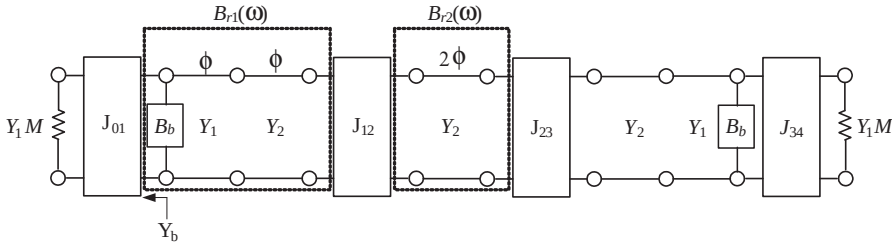

Figure 3. Equivalent circuit model of Figure 2(c).

In order to obtain the equivalent susceptances of the transmission line sections in Figure 3, the first and second transmission line sections are modeled in Figures 4(a) and (b). When $\omega \approx \omega_0$, the input impedances ($Z_{in,1}$ and $Z_{in,2}$) in Figure 4(a) are expressed as:

$$Z_{in,1} = Z_1 \frac{Z_1 + jZ_L \frac{\pi}{2}\left(\frac{\omega-\omega_o}{\omega_o}\right)}{Z_L + jZ_1 \frac{\pi}{2}\left(\frac{\omega-\omega_o}{\omega_o}\right)}\Bigg|_{\omega\approx\omega_o} \tag{9}$$

$$Z_{in,2} = Z_2 \frac{Z_2 + jZ_L \frac{\pi}{2}\left(\frac{\omega-\omega_o}{\omega_o}\right)}{Z_L + jZ_2 \frac{\pi}{2}\left(\frac{\omega-\omega_o}{\omega_o}\right)}\Bigg|_{\omega\approx\omega_o} \tag{10}$$

The input impedance of the second transmission line section in Figure 4(b) is then shown as:

$$Z_{in} = Z_2 \frac{Z_L + jZ_2\pi\left(\frac{\omega-\omega_o}{\omega_o}\right)}{Z_2 + jZ_L\pi\left(\frac{\omega-\omega_o}{\omega_o}\right)}\Bigg|_{\omega\approx\omega_o} \tag{11}$$

Since both ends of the lines in Figures 4(a) and (b) are physically open circuit, the condition, $Z_L \gg Z_1$ and $Z_L \gg Z_2$ could be applied to (9)–(11). As a result, using their admittance expressions, (9)–(11) can be simplified as:

$$Y_{in,1} = jY_1 \frac{\pi}{2}\left(\frac{\omega-\omega_o}{\omega_o}\right) = jB_1(\omega)|_{\omega\approx\omega_o} \tag{12}$$

$$Y_{in,2} = jY_2 \frac{\pi}{2}\left(\frac{\omega-\omega_o}{\omega_o}\right) = jB_2(\omega)|_{\omega\approx\omega_o} \tag{13}$$

$$Y_{in} = jY_2\pi\left(\frac{\omega-\omega_o}{\omega_o}\right) = jB_{r2}(\omega)|_{\omega\approx\omega_o} \tag{14}$$

B_1 and B_2 which are the input susceptances of the first line section in Figure 4(a) can be determined from (12) and (13). Total susceptance,

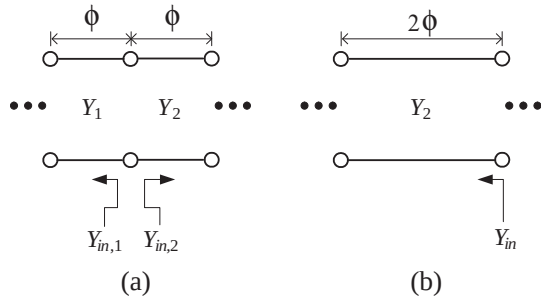

Figure 4. Modeling of the transmission line sections, (a) the first section, and (b) the second section.

B_{r1} of the first line section in Figure 3 can be obtained by adding B_b, B_1, and B_2. The equation in (14) presents the susceptance of the second line section in Figure 4(b).

Once the total susceptances (B_{r1} and B_{r2}) of the first and second line sections are found in Figure 3, their slope parameters can simply be determined by solving the first order differential equations in terms of ω:

$$b_{r1} = \frac{\omega_o}{2}\frac{dB_{r1}}{d\omega}\bigg|_{\omega=\omega_0} = \frac{\pi Y_1}{4}\left[\frac{J_{01}^2}{Y_1^2}\left(1-\frac{1}{M^2}\right)+\frac{Y_2}{Y_1}+1\right] \quad (15)$$

$$b_{r2} = \frac{\omega_o}{2}\frac{dB_{r2}}{d\omega}\bigg|_{\omega=\omega_0} = \frac{\pi}{2}Y_2 \quad (16)$$

Using (15) and (16), J-inverter expressions for the proposed BPFs in Figures 1(b) and (c) can be presented as:

$$J_{01} = J_{34} = \sqrt{\frac{WY_1M\pi\left(Y_1+Y_2\right)}{4g_0g_1 - W\pi\left(M-1/M\right)}} \quad (17)$$

$$J_{12} = J_{23} = \sqrt{\frac{W^2}{g_1g_2}\left[\frac{\pi^2Y_1Y_2}{8}\left\{\frac{J_{01}^2}{Y_1^2}\left(1-\frac{1}{M^2}\right)+\frac{Y_2}{Y_1}+1\right\}\right]} \quad (18)$$

In (15)–(18), $\omega_o = \frac{2\omega_2\omega_1}{\omega_2+\omega_1}$, $W = 2\left(\frac{\omega_2-\omega_1}{\omega_2+\omega_1}\right)$, $M = \frac{Y_1}{Y_0}$, and g = lowpass prototype element value.

Based on the new J-inverter equations in (17) and (18), the series capacitive susceptances and negative electrical lengths in Figure 2(b)

can be shown as:

$$B_{j,j+1} = \left.\frac{J_{j,j+1}}{1-\left(\frac{J_{j,j+1}}{Y_1}\right)^2}\right|_{j=0,1,\ldots,3} \tag{19}$$

$$\phi_{j,j+1} = \left.-\tan^{-1}\left(\frac{2B_{j,j+1}}{Y_1}\right)\right|_{j=0,1,\ldots,3} \tag{20}$$

Since $B_{01} = B_{34}$ and $B_{12} = B_{23}$ in Figures 2(a) and (b), electrical lengths of the proposed BPFs in Figures 1(b) and (c) are: $\theta_0 = \theta_{1,a} = \theta_{3,a} = \theta_4$ and $\theta_{1,b} = \theta_{3,b}$. Using the equations in (1), (2), (19), and (20), the electrical lengths of the proposed BPFs in Figures 1(b) and (c) can be calculated from:

$$\theta_0 = \frac{\pi - \tan^{-1}\left(\frac{2B_{0,1}}{Y_1}\right)}{2} \tag{21}$$

$$\theta_{1,b} = \frac{\pi - \tan^{-1}\left(\frac{2B_{1,2}}{Y_2}\right)}{2} \tag{22}$$

$$\theta_2 = \pi - \frac{1}{2}\left[\tan^{-1}\left(\frac{2B_{12}}{Y_1}\right) + \tan^{-1}\left(\frac{2B_{23}}{Y_1}\right)\right] \tag{23}$$

Using (19), actual series coupling capacitance values in Figure 2(a) can be determined by:

$$C_{j,j+1} = \left.\frac{B_{j,j+1}}{\omega_o}\right|_{j=0,\,1,\,\ldots,3} \tag{24}$$

3. VERIFICATION OF PROPOSED EQUATIONS

In order to validate the proposed design method, a capacitive gap-coupled BPF using non-uniform arbitrary image impedances is designed based on the derived equations. The simulated results are then compared with the calculated results. For the theoretical verifications, the BPF is designed on microstrip, where a substrate thickness and a dielectric constant are 0.508 mm and 2.2, respectively. The BPF's center frequency is 5.8 GHz and the FBW is set to 3.5%. The number of the filter stages is $N = 3$, and Chevyshev prototype element values for passband ripple of 0.01 dB have been used for the proposed J-inverter calculations. Based on the proposed equations, the BPF's electrical lengths and capacitance values are calculated from (17)–(24). Table 1 shows the resulting element values.

Figures 5(a)–(d) illustrate the frequency responses of the proposed BPF, where the arbitrary image impedance, Z_1 is set to $70\,\Omega$, and Z_2 varies from 80 to $60\,\Omega$. In Figures 5(a) and (b), a magnitude of passband return loss decreases as mismatch degree ($|Z_1–Z_2|$) becomes

Table 1. Calculated BPF element values for Figure 2(a).

	θ_0, $\theta_{1,a}$	$\theta_{1,b}$	θ_2	$C_{01} = C_{34}$	$C_{12} = C_{23}$
$Z_1 = 70$, $Z_2 = 80$	76.6859	85.9543	171.9086	0.0983	0.02439
$Z_1 = 70$, $Z_2 = 75$	76.4879	86.0221	172.0441	0.1001	0.02557
$Z_1 = 70$, $Z_2 = 65$	76.0141	86.1613	172.3225	0.1041	0.02846
$Z_1 = 70$, $Z_2 = 60$	75.7272	86.2328	172.4656	0.1066	0.03025
$Z_1 = 70$, $Z_2 = 70$	76.2656	86.0910	172.1821	0.1019	0.02692
$Z_1 = 50$, $Z_2 = 50$	73.6469	86.0339	172.0679	0.1762	0.03824

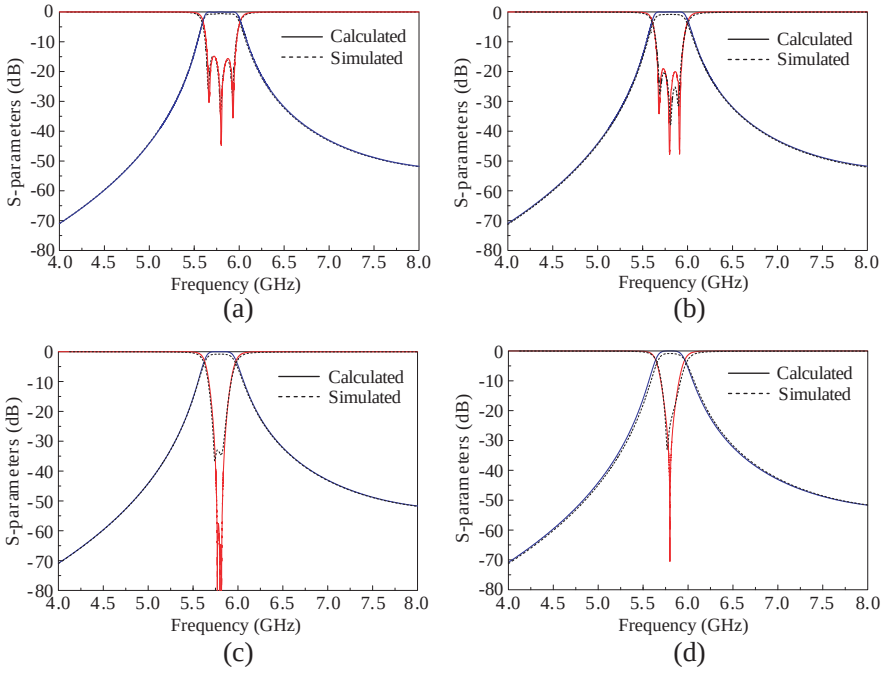

Figure 5. Calculated and simulated results of proposed capacitive gap-coupled BPF.

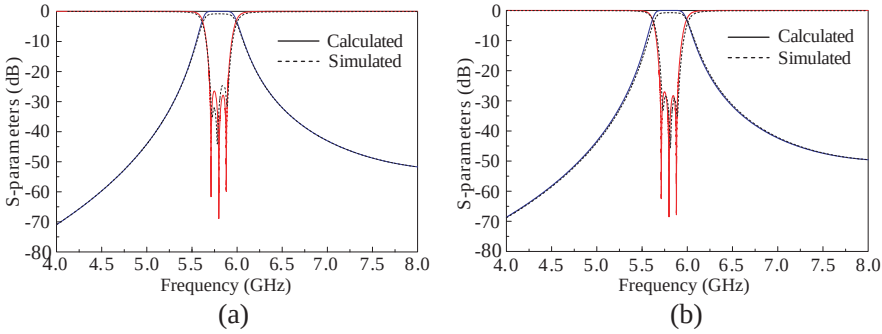

Figure 6. Calculated and simulated results of proposed capacitive gap-coupled BPF, (a) $Z_1 = 70$ and $Z_2 = 70\,\Omega$, and (b) $Z_1 = 50$ and $Z_2 = 50\,\Omega$.

higher. In this case ($Z_1 < Z_2$), the filter's bandwidth also increases as Z_2 becomes greater than Z_1. In (17) and (18), increasing Z_2 results in larger J-inverter values. Because J-inverter values are always less than a unity for a BPF design, a susceptance in (19) becomes larger. Therefore, a capacitance in (24) becomes greater As a result, increasing Z_2 produces a wide bandwidth due to a larger capacitance. In Figures 5(c) and (d), the magnitude of return loss in the passband increases as Z_2 becomes smaller than Z_1. However, in this case, a bandwidth of the BPF decreases. When Z_2 is further decreased in Figure 5(d), it is also observed that the designed BPF produces a single S_{11} pole in the passband. As mentioned earlier, the image impedances (Z_1 and Z_2) can arbitrarily be set by a designer, but input/output feed line characteristic impedances (Z_0) are fixed at $50\,\Omega$.

Figures 6(a) and (b) show the frequency responses when $Z_1 = Z_2$. In Figure 6(a), the arbitrary image impedances, Z_1 and Z_2 are set to $70\,\Omega$. This could be the uniform arbitrary image impedance design for a capacitive gap-coupled BPF. As shown in Figure 6(a), the design provides a return loss greater than 20 dB, and satisfies the desired design specifications, i.e., FBW, center frequency, and etc. In Figure 6(b), the arbitrary image impedances, Z_1 and Z_2 are set to $50\,\Omega$, which is identical to a conventional capacitive gap-coupled BPF. Both calculated and simulated results in Figures 6(a) and (b) show good agreement.

4. CONCLUSION

A capacitive gap-coupled BPF using non-uniform arbitrary image impedances has been introduced and studied based on circuit and classical filter theories. The proposed design topologies and equations are validated from comparing the equation based calculation results and simulated results. In the proposed design, two different impedances can arbitrarily be set to the image impedances of a capacitive gap-coupled line BPF. Therefore, a designer can favorably control the BPF's resonator characteristic impedances. This would allow of reasonable line widths and gap dimensions on a low or high dielectric constant substrate. Using the derived design equations, a capacitive gap-coupled BPF has been designed and simulated. Both calculated and simulated results have shown good agreement. The proposed design technique is simple and easy, and the design could be realized using a microstrip line or a suspended strip line.

ACKNOWLEDGMENT

This work is supported in part by National Science Foundation (NSF) under Grant ECCS-0901088. The author would like to thank Ming-Yi Li, Texas A&M University, College Station, for his helpful suggestions.

REFERENCES

1. Matthaei, G. L., L. Young, and E. M. T. Johns, *Microwave Filters, Impedance Matching Networks, and Coupling Structures,* Arthech House, Dedham, 1980.
2. Cohn, S. B., "Direct coupled resonator filters," *Proc. IRE*, Vol. 45, No. 2, 187–196, Feb. 1957.
3. Cohn, S. B., "Parallel-coupled transmission-line-resonator filters," *IRE Trans. Microw. Theory Tech.*, Vol. 6, No. 2, 223–231, Apr. 1958.
4. Ahn, D., C.-S. Kim, M.-H. Chung, D.-H. Lee, D.-W. Lew, and H.-J. Hong, "The design of parallel coupled line filter with arbitrary image impedance," *IEEE MTT-S Int. Microwave Symp. Dig.*, Vol. 2, 909–912, Jun. 1998.
5. Gan, H., D. Lou, and D. Yang, "Compact microstrip bandpass filter with sharp transition bands," *IEEE Microw. Wireless Compon. Lett.*, Vol. 16, No. 3, 107–109, Mar. 2006.

6. Ahn, D., J. S. Park, C. S. Kim, J. Kim, Y. Qian, and T. Itoh, "A design of the low-pass filter using the novel microstrip defected ground structure," *IEEE Trans. Microw. Theory Tech.*, Vol. 49, No. 1, 86–93, Jan. 2001.
7. Jung, D.-J. and K. Chang, "Low-pass filter design through the accurate analysis of electromagnetic-bandgap geometry on the ground plane," *IEEE Trans. Microw. Theory Tech.*, Vol. 57, No. 7, 1798–1805, Jul. 2009.
8. Kuo, T.-N., S.-C. Lin, and C. H. Chen, "Compact ultra-wideband bandpass filters using composite microstrip-coplanar waveguide structure," *IEEE Trans. Microw. Theory Tech.*, Vol. 54, No. 10, 3772–3778, Oct. 2006.
9. Jung, D.-J. and K. Chang, "Accurate modeling of microstrip dumbbell shaped slot resonator (DSSR) for miniaturized tunable resonator and band-pass filter," *Progress In Electromagnetics Research C*, Vol. 23, 137–150, 2011.
10. Makimoto, M. and S. Yamashita, "Bandpass filters using parallel coupled stripline stepped impedance resonators," *IEEE Trans. Microw. Theory Tech.*, Vol. 28, No. 12, 1413–1417, Dec. 1980.
11. Bonache, J., I. Gil, J. García-García, and F. Martín, "Novel microstrip band pass filters based on complementary split rings resonators," *IEEE Trans. Microw. Theory Tech.*, Vol. 54, 265–271, Jan. 2006.
12. Jung, D.-J., J.-K. Lee, and K. Chang, "Wideband banpass filter using microstrip ring," *Microw. Opt. Technol. Lett.*, Vol. 53, No. 1, 154–155, Jan. 2011.
13. Lim, J.-S., Y.-T. Lee, C.-S. Kim, D. Ahn, and S. Nam, "A vertically periodic defected ground structure and its application in reducing the size of microwave circuits," *IEEE Microw. Wireless Compon. Lett.*, Vol. 12, No. 12, 240–242, Dec. 2002.
14. Jung, D.-J. and K. Chang, "Microstrip diplexer design for X-band RF/microwave front-end applications," *IEEE Int. Symp. on Antennas and Propag.*, 5–7, Aug. 2011.
15. Ting, S.-W., K.-W. Tam, and R. P. Martins, "Miniaturized microstrip lowpass filter with wide stopband using double equilateral U-shaped defected ground structure," *IEEE Microw. Wireless Compon. Lett.*, Vol. 16, No. 5, 240–242, May 2006.
16. Wang, X.-H., B.-Z. Wang, and K. J. Chen, "Compact broadband dual-band bandpass filters using slotted ground structure," *Progress In Electronmagnetics Research*, Vol. 82, 151–166, 2008.